Loss of the cleaved-protamine 2 domain leads to incomplete histone-to-protamine exchange and infertility in mice

Lena Arévalo[1], Gina Esther Merges[1], Simon Schneider[1], Franka Enow Oben[1], Isabelle Neumann[1], Hubert Schorle[1]

[1] Department of Developmental Pathology, Institute of Pathology, University Hospital Bonn, Germany

Corresponding author: lena.arevalo@ukbonn.de, schorle@uni-bonn.de

Keywords: Protamines, PRM2 processing, chromatin, chromatin condensation, sperm, spermiogenesis, histone retention, protamine ratio

Abstract

Protamines are unique sperm-specific proteins that package and protect paternal chromatin until fertilization. A subset of mammalian species expresses two protamines (PRM1 and PRM2), while in others PRM1 is sufficient for sperm chromatin packaging. Alterations of the species-specific ratio between PRM1 and PRM2 are associated with infertility. Unlike PRM1, PRM2 is generated as a precursor protein consisting of a highly conserved N-terminal domain, termed cleaved PRM2 (cP2), which is consecutively trimmed off during chromatin condensation. The carboxyterminal part, called mature PRM2 (mP2), interacts with DNA and together with PRM1, mediates chromatin-hypercondensation. The removal of the cP2 domain is believed to be imperative for proper chromatin condensation, yet, the role of cP2 is not yet understood. We generated mice lacking the cP2 domain while the mP2 is still expressed. We show that the cP2 domain is indispensable for complete sperm chromatin protamination and male mouse fertility. cP2 deficient sperm show incomplete PRM2 incorporation, resulting in a severely altered protamine ratio, retention of transition proteins and aberrant retention of the testis specific histone variant H2A.L.2. During epididymal

29 transit, cP2 deficient sperm seem to undergo ROS mediated degradation leading to complete
30 DNA fragmentation. The cP2 domain therefore seems to be a key aspect in the complex
31 crosstalk between histones, transition proteins and protamines during sperm chromatin
32 condensation. Overall, we present the first step towards understanding the role of the cP2
33 domain in paternal chromatin packaging and open up avenues for further research.
34

35 **Introduction**

36 Chromatin structure and dynamics in the sperm nucleus are as unique as the sperm cell
37 itself, and are of major importance to sperm function, fertilizing ability, and embryo survival.
38 Paternal DNA is particularly vulnerable to damage, especially to oxidative stress during
39 epididymal sperm maturation and migration, leading to a higher requirement for protection
40 (Chen et al. 2002). At the same time, the size and shape of the sperm cell nucleus needs to
41 be optimized for efficient sperm movement through the female reproductive tract (Tourmente
42 et al. 2011). This is achieved by the complete reorganization of paternal chromatin from
43 nucleo-histone to nucleo-protamine during the final steps of spermatogenesis (Balhorn 2007,
44 Rathke et al. 2014).
45 Even though many studies have demonstrated that the correct execution of this transition is
46 imperative for male fertility and embryo survival (Aoki and Carrell 2003), surprisingly little is
47 known about the process itself. Recent studies have only just started to unravel its molecular
48 basis (Schneider et al. 2016, Barral et al. 2017, Hada et al. 2017). Barral et al. (2017) were
49 able to show that the testis specific histone variant H2A.L.2 together with TH2B and
50 transition proteins (TNP1 and TNP2) mediates structural changes in chromatin allowing
51 protamines to bind DNA. Protamines are small, arginine-rich proteins. Their high arginine
52 content allows them to bind DNA with high affinity and to shield the charges of the DNA
53 backbone more efficiently than histones (Balhorn 1989, Tanaka and Baba 2005). Two types
54 of protamines have been identified in mammals: protamine 1 (*PRM1*, PRM1) and protamine
55 2 (*PRM2*, PRM2). While PRM1 is a major sperm protamine found across mammals, PRM2 is
56 only detected in the sperm of primates, most rodents, and a subset of other placental

57 mammals (Chauviere et al. 1992, Retief and Dixson 1993). The coding regions of *PRM1* and
58 *PRM2* are tightly clustered and map to a small section of chromosome 16. It is highly likely
59 that *PRM2* is the result of a *PRM1* duplication event (Krawetz and Dixon 1988, Lüke et al.
60 2011).
61 Unlike PRM1, PRM2 is transcribed as a precursor. The N-terminal region of the translated
62 PRM2, termed cleaved-PRM2 (cP2), is successively cleaved over several days while
63 chromatin condensation is taking place. After this, only mature-PRM2 (mP2) remains bound
64 to the completely condensed DNA (Retief et al. 1993, Balhorn 2007, Yelick et al. 1987, Oliva
65 and Dixon 1991). Perturbations of PRM2 processing has been shown to lead to decreased
66 DNA integrity and sperm dysfunction (deYebra et al. 1998, Torregrosa et al. 2006). In
67 previous comparative evolutionary studies, it was shown that the cP2 coding sequence is
68 conserved in both primates and rodents. mP2, however, evolves under less selective
69 constraint (Lüke et al. 2011, 2016). Changes in coding sequences of cP2 were associated
70 with differences in sperm head size in mouse species. This association was specific to the
71 cP2 domain and not found for mP2 (Lüke et al. 2014a). A potential reason for this pattern is
72 that changes in cP2 are selected against conserving a crucial function for reproduction, while
73 mP2 is free to evolve under less constraint due to its proposed functional redundancy to
74 PRM1 (Lüke et al. 2011, 2016).
75 Proper PRM2 cleaving therefore seems to be crucial for successful reproduction, yet, the
76 function of the cP2 domain and PRM2 processing are unknown to date. Establishment and
77 analysis of PRM2 deficient mice revealed that $Prm2^{-/-}$ males were infertile, while $Prm2^{+/-}$
78 males remained fertile (Schneider et al. 2016). Of note, mice deficient for TNP1, TNP2 and
79 H2A.L.2 show incomplete PRM2 processing (PRM2 precursor detected in mature sperm
80 nuclei) (Yu et al. 2000, Zhao et al. 2001, 2004, Barral et al. 2017).
81 Given that cP2 cleaving is taking place during DNA condensation in late spermiogenesis, the
82 strong evolutionary conservation of this domain and the effect of incomplete PRM2
83 processing on sperm function and fertility, cP2 is likely to play an important role in the correct
84 execution of chromatin condensation. We therefore studied the involvement of cP2 in

85 chromatin condensation during spermiogenesis by generating and analyzing a mouse line
86 bearing a deletion of cP2, while maintaining mP2 expression. We analyzed fertility, testis and
87 sperm morphology, chromatin integrity and nuclear protein content of these mice and
88 revealed that Prm2$^{\Delta c/+}$ mice are already infertile and that cP2 seems necessary for complete
89 protamination of sperm chromatin.
90
91 **Material and Methods**
92 Animals
93 For the generation of mouse lines using CRISPR/Cas9 the F1 generation of mouse strains
94 C57Bl6 and DBA2 (B6D2F1) were used. Founder animals were backcrossed to C57Bl6.
95 Mice were maintained under standard laboratory conditions in environmentally controlled
96 rooms (20–24ºC) on a 12L:12D photoperiod with nesting material and ad libitum food and
97 water. All animal experiments were conducted according to German law of animal protection
98 and in agreement with the approval of the local institutional animal care committees
99 (Landesamt für Natur, Umwelt und Verbraucherschutz, North Rhine-Westphalia, Germany,
100 AZ81-02.04.2018.A369).
101
102 Gene-edited mouse lines
103 Guide RNA (gRNA) sequence pre-selection was performed using the algorithm published by
104 Hsu et al. (2013). Two gRNA sequences were selected based on quality scores in each case
105 maximizing specificity and minimizing off-target action (score > 50) (Table S1). The designed
106 guide sequences were ordered as crisprRNA sequences (crRNA) (IDT, Leuven, Belgium)
107 and annealed to tracrRNA (IDT) by incubating 5min at 95°C for a final concentration of 50mM
108 of gRNA (crRNA+tracrRNA). The target site of the designed gRNAs is shown in figure S1A.
109 The repair template used for homology directed repair (HDR), here single-stranded
110 oligodeoxynucleotides (ssODNs) (IDT) (Yoshimi et al. 2014, 2016), are shown in figure S1B.
111 Ribonucleoprotein (RNP) complexes were assembled immediately prior to delivery by
112 incubation of 4pmol/µl Cas9 (IDT) protein, 4pmol/µl of each gRNA and 10pmol/µl ssODN in

113 Opti-MEM medium (Thermo Fisher Scientific, Waltham, USA) for 10min at room
114 temperature.
115 To generate gene-edited founder animals, B6D2F1 females were hormonally superovulated
116 and mated as described (Schneider et al. 2016). Oocytes were isolated from the oviducts,
117 washed and transferred into droplets of Opti-MEM medium containing the previously
118 prepared RNP complex and electroporated using a BioRad Gene Pulser (BioRad,
119 Feldkirchen, Germany) (two 3ms square wave pulses at 30V with an 100ms interval).
120 Oocytes were recovered and washed 5x in M2 medium (Merck Millipore, Darmstadt,
121 Germany) followed by 3 washes in KSOM (Merck Millipore) medium droplets. Oocytes were
122 then incubated in KSOM medium covered in paraffin oil overnight at 37°C. Developing 2-cell
123 stage embryos were then transferred into the oviducts of pseudo-pregnant foster mice.
124 Offspring was genotyped (primers, see Fig. 1A, Table S1) and positive founder animals
125 backcrossed to C57Bl/6J for at least 3 generations before analysis. Male mice between 10
126 and 13 weeks of age were used for analysis.
127
128 Fertility analysis
129 Five males per genotype were mated with C57Bl/6J females 1:2 and females were checked
130 daily for the presence of a vaginal plug until at least 5 plugs per male were observed.
131 Pregnancy rate and litter size were noted.
132
133 Sampling and mature sperm isolation
134 The testes were dissected and weighed. For paraffin sectioning, testes and epididymides
135 were fixed in either Bouin's solution for histology or in 4% Paraformaldehyde solution for
136 immunohistochemistry (IHC). For tubule preparations testes were transferred to PBS and
137 tubules dissected as described in Kotaja et al. (2004). Briefly, tubules were separated and
138 elongating and condensed spermatid containing sections were identified through their light
139 absorption pattern using a dissection microscope. Tubule sections were squashed on a slide,
140 frozen in liquid nitrogen for 20 seconds, fixed in 90% ethanol for 5 minutes and air dried.

141 Tubule preparations were used for IHC. To obtain sperm samples, caudae epididymes were
142 dissected and transferred to preheated (36-37°C) M2 medium, incised several times,
143 squeezed with tweezers several times during a 30min incubation period at 36-37°C to ensure
144 flushing out the whole sperm population including immotile sperm.
145
146 Histology
147 Bouin-fixed testes and epididymes were paraffized, embedded in paraffin blocks and
148 sectioned at 3 microns. Sections were deparaffinized and stained with the Periodic acid–
149 Schiff (PAS) procedure. Stained sections were imaged under bright field at 20x and 63x
150 magnification using a Leica DM5500 B microscope (Leica Microsystems, Wetzlar, Germany).
151
152 Basic sperm analysis
153 Isolated spermatozoa were counted for 6-12 animals per genotype using a hemocytometer.
154 Sperm motility was analyzed for 3-4 animals per genotype by taking 5-10, 3 second video
155 clips per animal using a Basler acA1920-155ucMED camera (Basler AG, Ahrensburg,
156 Germany). A minimum of 200 sperm per individual were analyzed and the percentage of
157 motile sperm calculated. Sperm viability was analyzed by eosin-nigrosin staining for 3-4
158 animals per genotype. Approximately 1 x 10^6 sperm were mixed with 50µl of eosin-nigrosin
159 dye, incubated for 30 seconds, spread on slides, air-dried and cover-slipped. A minimum of
160 200 spermatozoa were analyzed under bright field (Leica DMIRB microscope) and the
161 percentage of viable spermatozoa calculated.
162
163 RNAseq and differential expression analysis
164 RNA was extracted from testes after removal of the tunica albuginea using the RNeasy kit
165 (Qiagen, Hilden, Germany). RNA integrity (RIN) was determined using the RNA Nano 6000
166 Assay Kit with the Agilent Bioanalyzer 2100 system (Agilent Technologies, Santa Clara, CA,
167 USA). RIN values ranged from 7.3–10 for all samples. RNA sample quality control and library
168 preparation were performed by the University of Bonn Core facility for Next Generation

169 Sequencing (NGS), using the QuantSeq 3'-mRNA Library Prep (Lexogen, Greenland, NH,
170 USA). RNAseq was performed by the University of Bonn Core facility for Next Generation
171 Sequencing (NGS) on the Illumina HiSeq 2500 V4 platform, producing >10 million, 50bp 3'-
172 end reads per sample.
173 The samples were then mapped to the mouse genome (GRCm38.89) using HISAT2 2.1 (Kim
174 et al. 2015). StringTie 1.3.3 (Pertea et al. 2015) was used for transcript quantification and
175 annotation. Gene annotation was retrieved from the Ensembl FTP server
176 (ftp://ftp.ensembl.org)(GRCm38.89). The python script (preDE.py) included in the StringTie
177 package was used to prepare DEseq2-compatible gene-level count matrices for analysis of
178 differential gene expression. Mapping to the *Prm2* genomic location was visualized using the
179 Integrative Genomics Viewer (IGV; Robinson et al. 2011).
180 Differential expression (DE) was analyzed using DESeq2 1.16.1 (Love et al. 2014). The
181 adjusted p-value (Benjamini-Hochberg method) cutoff for DE was set at < 0.05, log2 fold
182 change of expression (LFC) cutoff was set at > 1. We performed GO term and pathway
183 overrepresentation analyses on relevant lists of genes using the PANTHER gene list analysis
184 tool with Fisher's exact test and FDR correction (Mi et al. 2017).
185
186 Sperm nuclear morphology
187 Nuclear morphology was analyzed for 3 individuals per genotype. Approximately 1.5 x 10^6
188 sperm were fixed in methanol-acetic acid (3:1), spread onto a slide and stained with 4′,6-
189 diamidino-2-phenylindole (DAPI) nuclear stain (ROTI®Mount FluorCare DAPI (Carl Roth
190 GmBH, Karlruhe, Germany)). At least 200 stained sperm cells per individual were imaged at
191 100x magnification using a Leica DM5500 B fluorescent microscope. Nuclear morphology
192 was analyzed using the stand-alone version of the Nuclear Morphology program by Skinner
193 et al. (2019). The program allows for automated detection and morphological analysis of
194 mouse sperm nuclei (among other species and cell types). It additionally provides options for
195 clustering heterogenous populations by nuclear parameters and comparative analyses of

196 nuclear morphology (Skinner et al. 2019). The parameters used for nucleus detection are
197 shown in figure S3.
198
199 Sperm basic nuclear protein extraction and analysis
200 Basic nuclear proteins were extracted described in Soler-Ventura et al. (2018). Briefly,
201 approximately 10 x 10^6 of swim-out sperm were washed in PBS and pelleted. The pellet was
202 resuspended in buffer containing 1M Tris pH 8, 0.5M MgCl and 5ul Triton X-100.
203 Subsequently the pellet was treated with 1mM PMSF in water inducing cell lysis. Treatment
204 with EDTA, DTT and GuHCl induced DNA denaturation. Incubation at 37°C for 30min in
205 presence of 0.8% vinylpyridine is necessary for mouse protamine separation on the
206 subsequent protein gel. DNA is then precipitated by addition of EtOH and separated from the
207 sample by centrifugation. Basic sperm nuclear proteins are then extracted and dissolved in
208 0.5M HCl, followed by protein precipitation with TCA, acetone washes and drying. The
209 precipitated proteins are resuspended in sample buffer containing 5.5 M urea, 20% β-
210 mercapto-ethanol and 5% acetic acid.
211 The samples were then run on a pre-electrophorized acid-urea polyacrylamide gel (AU-
212 PAGE) (2.5 M urea, 0.9 M acetic acid, and 15% acrylamide/0.1% N,N′-Methylene bis-
213 acrylamide, TEMED and APS). The extracted basic nuclear proteins migrate towards the
214 negative pole at a 150V for 1h, 50min. The gels were stained with Coomassie Brilliant Blue
215 (Sigma Aldrich, Taufkirchen, Germany) using standard procedures. The two main protamine
216 bands can be observed in the bottom of the gel with mature-PRM2 corresponding to the
217 upper and PRM1 the lower band (Ishibashi et al. 2010, Soler-Ventura et al. 2018). PRM2
218 precursor bands can be observed in the lower part of the gel above the mature-PRM2 band,
219 if present (Yu et al. 2000, de Mateo et al. 2011). In the upper half of the gel, bands
220 corresponding to other basic nuclear proteins, including histones can be found (see Soler-
221 Ventura 2018). The densities of Coomassie stained bands were analyzed using ImageJ
222 (1.52k, Schneider et al. 2012).
223

224 Immunohistochemistry

225 PFA fixed testis and epididymis sections as well as EtOH fixed tubule preparations were
226 used for immunofluorescent staining. Sections were deparaffinized in xylol and rehydrated.
227 Sections and tubule preparations were washed in PBS and blocked for 30 min with normal
228 horse serum (Vectorlabs, Burlingame, USA) at room temperature, followed by primary
229 antibody incubation over night at 4°C. Antibodies and dilutions are shown in table S3. Slides
230 were then double-stained with fluorescent secondary antibodies using the VectaFluor™ Duet
231 Immunofluorescence Double Labeling Kit, DyLight® 594 Anti-Rabbit (red), DyLight® 488
232 Anti-Mouse (green) (Vectorlabs, Burlingame, USA), DAPI counterstained and coverslipped
233 with ProLong™ Gold antifade reagent with DAPI (Thermo Fisher Scientific, Waltham, USA).
234

235 Mass spectrometry and differential protein abundance analysis

236 Basic nuclear protein extractions were done for 3 individuals per genotype using
237 approximately 10^6 sperm. Extracted proteins were dissolved in sample buffer (5.5 M urea,
238 20% β-mercapto-ethanol and 5% acetic acid).
239 Peptide preparation: Protein solutions (5.5 M urea, 20% 2-mercaptoethanol, 5% acetic acid)
240 were dried in a vacuum concentrator and subjected to in solution preparation of peptides.
241 Proteins were dissolved in 50 mM acrylamide solution (Tris-HCl, pH=8) and alkylated for 30
242 min at RT. 1 µg of Trypsin were added for o/n proteolysis at 37°C. Dried peptides were
243 dissolved in 10 µL 0.1% trifluoro acetic acid (TFA) and desalted with ZipTips (Waters GmbH,
244 Eschborn, Germany) according to standard solid-phase extraction procedures. Equilibration
245 and binding was done in presence of 0.1% TFA, washing with 0.1% formic acid (FA). Eluates
246 (50% acetonitrile, 0.1% FA) were dried and stored at -20°C.
247 LC-MS measurements: Peptide separation was performed on a Dionex Ultimate 3000 RSLC
248 nano HPLC system (Dionex GmbH, Idstein, Germany). The autosampler was operated in µl-
249 pickup mode. Peptides were dissolved in 10 µl 0.1% FA (solvent A). 2 µL were injected onto
250 a C18 analytical column (300 mm length, 75 µm inner diameter, ReproSil-Pur 120 C18-AQ,
251 1.9 µm). Peptides were separated during a linear gradient from 2% to 35% solvent B (90%

252 acetonitrile, 0.1% FA) within 90 min at 300 nl/min. The nanoHPLC was coupled online to an
253 Orbitrap Fusion Lumos mass spectrometer (Thermo Fisher Scientific, Bremen, Germany).
254 Peptide ions between 300 and 1600 m/z were scanned in the Orbitrap detector every 3
255 seconds with R=120,000 (maximum fill time 50 ms, AGC target 400,000). Polysiloxane
256 (445.12002 Da) was used for internal calibration (typical mass error ≤1.5 ppm). In a top-
257 speed method peptides were subjected to higher energy collision induced dissociation (HCD:
258 1.0 Da isolation, threshold intensity 25,000, normalized energy 27%) and fragments analyzed
259 in the Orbitrap with target 50,000 and maximum injection time 22 ms, R=15,000. Fragmented
260 peptide ions were excluded from repeat analysis for 20 s.
261 Data analysis: Raw data processing and was performed with Proteome Discoverer software
262 2.5.0.400 (Thermo Fisher Scientific). Peptide identification was done with an in-house
263 Mascot server version 2.6.1 (Matrix Science Ltd, London, UK). MS data were searched
264 against *Mus musculus* sequences from SwissProt (2021/03, including isoforms), and
265 contaminants (cRAP, Mellacheruvu et al. 2013). Precursor Ion m/z tolerance was 10 ppm,
266 fragment ion tolerance 20 ppm. Tryptic peptides with up to two missed cleavages were
267 searched. Propionamide on cysteines was set as static modification. Oxidation was allowed
268 as dynamic modification of methionine, acetylation as modification of protein N-termini.
269 Mascot results were evaluated by the percolator algorithm (Kall et al. 2008) version 3.05 as
270 implemented in Proteome Discoverer. Spectra with identifications below 1% q-value were
271 sent to a second round of database search with semitryptic enzyme specificity (one missed
272 cleavage allowed). Protein N-terminal acetylation, methionine oxidation, carbamylation on
273 lysine and N-termini were allowed as dynamic modifications. Actual FDR values were
274 typically ≤0.5% (peptide spectrum matches), ≤1.0% (peptides), <1% (proteins). Proteins were
275 accepted if at least two peptides with q-value <1% were identified. Summed abundances
276 (areas of precursor extracted ion chromatograms of unique peptides) were used for relative
277 quantification.
278 Differential abundance (DA) analysis: DA analysis was performed using the Bioconductor
279 package proDA (Ahlmann-Eltze C 2021) using peptide spectrum matches (PSM) level data

280 extracted from Protein Discoverer. Only proteins detected in all genotypes and all replicates
281 with more than two peptides were included in the analysis. The data were log2 transformed
282 and median normalized prior to DA analysis to ensure comparability. The proDA package is
283 based on linear models and utilized Bayesian priors to increase power for differential
284 abundance detection (Ahlmann-Eltze C 2021). Proteins with a log2 fold change (LFC) of >1
285 and false discovery rate adjusted p-value (FDR) <0.05 were considered differentially
286 abundant compared to the WT. Plots were generated using the R-package ggplot2 (Wickam
287 2016).
288
289 Generation of expression plasmids and transfection
290 *Prm2* and Prm2$^{\Delta c}$ cDNA (GenBank: NM_008933.2) was amplified from C57Bl6 mouse testis
291 cDNA using overhang primers introducing suitable restriction enzyme motifs (table S1) and
292 cloned N-terminally in-frame with eGFP into the pEGFP-N3 vector (6080-1). Correct
293 sequence and insertion were verified by sequencing.
294 Human Embryonic Kidney 293 (HEK293) cells were cultured in standard medium (DMEM,
295 10% FBS). HEK293 cells were transfected at 80% confluence with 3 µg of pPrm2-EGFP-N3
296 (*Prm2*), pPrm2$^{\Delta c}$-EGFP-N3 (Prm2$^{\Delta c}$ sequence) or pEGFP-N3 with FuGENE® HD
297 Transfection Reagent (Promega, Madison, USA), according to the manufacturer's
298 instructions. At 12 hours post-transfection the medium was changed. Pictures were taken
299 after 48 hours using a Leica DMIRB inverted microscope (Leica Microsystems, Wetzlar,
300 Germany).
301
302 **Results**
303 Generation of gene-edited mouse lines
304 To delete cP2 in the reading frame of the PRM2 gene, we used CRISPR/Cas9 with
305 templates catalyzing homology directed repair (HDR). In order to induce the deletion, we
306 used two gRNAs targeting the 5' and 3' ends of the cP2 domain (Fig. 1A, Fig. S1). A single
307 stranded DNA template encoding the 5' and 3' areas flanking the cP2 coding region enabling

308 deletion of the cP2 coding region and an in-frame repair, generating an allele, where only
309 mature PRM2 is expressed from the endogenous promoter, was added to the gene-editing
310 reaction (Fig. S1). The sequence of the generated allele, named Prm2$^{\Delta c}$, is shown in figure
311 S1A and was registered with the mouse genomics database (MGI:6718282). Animals were
312 generated, sequence validated and backcrossed to C57Bl/6J for at least 3 generations
313 before analysis.
314
315 <u>Prm2$^{\Delta c/+}$ as well as Prm2$^{\Delta c/-}$ male mice are infertile</u>
316 First, we subjected the Prm2$^{\Delta c/+}$ mice to a fertility test. Five Prm2$^{\Delta c/+}$ male mice were mated to
317 ten WT females and the pregnancy/litters were recorded for five confirmed vaginal plugs per
318 male (successful matings). We found that Prm2$^{\Delta c/+}$ male mice were infertile, with no observed
319 pregnancies in at least five confirmed matings each. This is in contrast to the deletion of the
320 entire PRM2 gene, where Prm2$^{+/-}$ male mice remained fertile (Schneider et al. 2016) (Fig.
321 1B). We hypothesized that an aberrant interaction between the newly generated mP2 and
322 the PRM2 precursor expressed from the wildtype allele might lead to interference and be
323 causative for infertility in these males. In order to test this, we bred Prm2$^{\Delta c/+}$ females with
324 Prm2$^{+/-}$ males published by us (Prm2$^{\Delta 97bp}$; Schneider et al. 2016, MGI:5760133) to generate
325 Prm2$^{\Delta c/-}$ mice. This results in male mice, in which only Prm2$^{\Delta c}$ is present and expressed.
326 However, Prm2$^{\Delta c/-}$ males did not produce any litters in at least five confirmed matings each
327 and can be considered infertile (Fig. 1B). This strongly suggests, that the cP2 domain is
328 essential for murine spermiogenesis. If cP2 was non-essential these Prm2$^{\Delta c/-}$ mice should be
329 fertile, similar to Prm2$^{+/-}$ males.
330
331 <u>mP2 is expressed in Prm2$^{\Delta c/-}$ mice and transcriptional silencing does not seem to be</u>
332 <u>disrupted</u>
333 Since the Prm2$^{\Delta c/-}$ mice allow for detection and validation of mP2 transcripts from the Prm2$^{\Delta c}$
334 allele we, performed RNAseq on testis samples and analyzed expression of *Prm2*. By
335 mapping the RNAseq reads to the *Prm2* genomic location, we were able to verify that the

336 mP2 transcript was indeed expressed from the gene edited Prm2$^{\Delta c}$ allele (Fig. S2). The
337 expression levels of the *Prm2* transcripts were comparable in all genotypes (WT, Prm2$^{\Delta c/+}$
338 and Prm2$^{\Delta c/-}$), thus the alleles do not display a gene dosage effect (Fig. 1C).
339 In our previous study we found that in the Prm2$^{-/-}$ testis, a much higher number of genes was
340 differentially higher than lower expressed (81:13) indicating incomplete protamine-mediated
341 transcriptional silencing (Schneider et al. 2020). Here, compared to WT, we found 36 genes
342 differentially higher expressed and 42 genes differentially lower expressed for Prm2$^{\Delta c/+}$ males
343 and 26 genes differentially higher and 43 differentially lower for Prm2$^{\Delta c/-}$ (Fig. 1D). This
344 indicates that transcriptional silencing is not notably disrupted in males harboring the Prm2$^{\Delta c}$
345 allele. No GO-term or pathway enrichment was found for analyzed gene sets. Lists of
346 differentially expressed genes and statistics can be found in supplementary dataset S1.
347
348 <u>mP2 is detected in Prm2$^{\Delta c/+}$ and Prm2$^{\Delta c/-}$ spermatid nuclei, but is also found in cytoplasm and</u>
349 <u>residual bodies</u>
350 After confirming, that the gene-edited mP2-domain is expressed from the Prm2$^{\Delta c}$ allele, we
351 next addressed the question, whether mP2 can be detected in spermatids and is able to
352 condense DNA. We therefore first performed IHC on PFA fixed testis sections. The epitope
353 of the PRM2 antibody (Hup2B, Briarpatch Bio, Livermore, USA) is located in the first half of
354 the mP2 domain and is able to detect both, the PRM2 protein generated from the wildtype
355 and the gene-edited Prm2$^{\Delta c}$ allele. As shown in figure 2A, PRM2 is detected in condensed
356 spermatid nuclei of Prm2$^{\Delta c/+}$ and Prm2$^{\Delta c/-}$ males, similar to the wildtype. However, we
357 additionally detected a signal in the cytoplasm of spermatids and residual bodies that is
358 strongest in Prm2$^{\Delta c/-}$ males and not found in wildtype (Fig. 2A).
359 To determine if mP2 is able to condense DNA, we expressed PRM2 and the mP2 sequence
360 of the Prm2$^{\Delta c}$ allele tagged with eGFP in HEK293 cells. The ability of PRM1 to bind to DNA
361 and condense nuclei when expressed *in vitro* in somatic cells had been demonstrated before
362 by Iuso et al. (2015) in sheep fibroblasts. Experiments revealed that PRM2-eGFP and

363 Prm2$^{\Delta c}$-eGFP locate to the HEK293 cell nuclei and are present after 48h as large speckles in
364 the nucleus (Fig. 2B). We therefore concluded that mP2 is able to condense the nucleus of
365 somatic cells *in vitro* and should therefore be able to contribute to spermatid chromatin
366 condensation *in vivo*.
367
368 Testis histology is inconspicuous, while mature sperm are inviable and immotile in Prm2$^{\Delta c/+}$
369 and Prm2$^{\Delta c/-}$ male mice
370 Next, we analyzed testis mass and examined histological sections to determine the nature of
371 the infertility. Relative testes mass did not differ from the wildtype (Fig. 3A). Almost no viable
372 and motile mature sperm were found in Prm2$^{\Delta c/+}$ and Prm2$^{\Delta c/-}$ males (Mean percent viable:
373 Prm2$^{\Delta c/+}$=1.7, SD=1.31; Prm2$^{\Delta c/-}$=0; Mean percent motile: Prm2$^{\Delta c/+}$=0.2, SD=0.45; Prm2$^{\Delta c/-}$
374 =0.25, SD=0.5) (Fig. 3A, Fig. S4). Interestingly, sperm count is significantly reduced in
375 Prm2$^{\Delta c/-}$ but not in Prm2$^{\Delta c/+}$ males compared to the wildtype (ANOVA: $F(2)=10.87$, $p<0.001$;
376 Post-hoc Tukey HSD: WT vs. Prm2$^{\Delta c/+}$: $p=0.89$, WT vs. Prm2$^{\Delta c/-}$: $p<0.001$) (Fig. 3A). To
377 determine if the loss of cP2 affects spermiogenesis, testis and epididymis histology was
378 evaluated by PAS staining of Bouin-fixed sections. Testis histology was inconspicuous and
379 spermatogenesis seemed not to be affected in either genotype (Fig. 3B). Epididymis
380 histology however, shows larger round cells and vacuole-like structures, which are indicative
381 of spermatid degradation. This was more pronounced in Prm2$^{\Delta c/-}$ males compared to Prm2$^{\Delta c/+}$
382 males (Fig. 3B).
383
384 Chromatin integrity is strongly affected and nuclear morphology is altered in Prm2$^{\Delta c/+}$ and
385 Prm2$^{\Delta c/-}$ male mice.
386 Since protamines condense sperm chromatin and were shown to influence sperm head
387 morphology (Lüke et al. 2014a,b), mature sperm DNA integrity and nuclear morphology
388 could be affected even though mP2 is able to condense DNA. We therefore extracted DNA
389 from mature sperm and subjected it to agarose gel electrophoresis. DNA from sperm of
390 Prm2$^{\Delta c/+}$ males is completely fragmented (Fig. 4A). Schneider et al. (2020) was able to show

391 that during epididymal transit, Prm2$^{-/-}$ deficient sperm underwent ROS mediated destruction,
392 leading to DNA and membrane degradation and immotility. We therefore stained sections of
393 epididymides against 8-Oxo-2'-deoxyguanosine (8-OHdG), which indicates oxidative DNA
394 damage. In the caput epididymis we detected only a slight increase of the 8-OHdG signal in
395 Prm2$^{\Delta c/+}$ and Prm2$^{\Delta c/-}$ males compared to the wildtype. However, in the Prm2$^{\Delta c/+}$cauda
396 epididymis a strong increase in 8-OHdG was visible compared to the wildtype. The 8-OHdG
397 signal in the Prm2$^{\Delta c/-}$ cauda was less intense, which is likely due to the more severe
398 degradation and reduced sperm count (Fig. 4B).
399 Nuclear morphology analysis revealed aberrant nuclear morphology of mature sperm in
400 Prm2$^{\Delta c/+}$ and Prm2$^{\Delta c/-}$ males. Sperm from both genotypes show a significantly reduced
401 nuclear size compared to the WT (Table S2, Fig. 4C, Fig. S5). Prm2$^{\Delta c/+}$ males show two
402 clusters of nuclear shape, a slimmer nucleus with decreased hook curvature and a smaller
403 hookless nucleus. This phenotype is even more severe in Prm2$^{\Delta c/-}$ males (Table S2, Fig. 4C,
404 Fig. S5). Of note, nuclear morphology of Prm2$^{\Delta c/-}$ and Prm2$^{\Delta c/+}$ deficient sperm also differs
405 from Prm2$^{+/-}$ and Prm2$^{-/-}$ males.
406
407 <u>The protamine ratio is flipped in Prm2$^{\Delta c/+}$ and Prm2$^{\Delta c/-}$ males</u>
408 Since the ratio between PRM1 and PRM2 is constant in mature sperm (in mice ~60%
409 PRM2), and alterations of this ratio are associated with sperm defects and infertility (Corzett
410 et al. 2002, Steger et al. 2008; García-Peiró et al. 2011), we next tested if male mice
411 harbouring the Prm2$^{\Delta c}$ allele display alterations of the PRM1/PRM2 ratio. Interestingly, acid-
412 urea gel electrophoresis (AU-PAGE) of mature sperm basic nuclear proteins showed several
413 bands corresponding to PRM2 precursors in Prm2$^{\Delta c/+}$ males. This was also the case in
414 Prm2$^{+/-}$ males.
415 Comparing the densities of the PRM1 band relative to mP2 and PRM2 precursor bands, we
416 found the PRM ratio to be strongly altered, showing a lower percentage of PRM2 (including
417 precursors) compared to the wildtype in Prm2$^{\Delta c/+}$ and Prm2$^{\Delta c/-}$ males (Mean %PRM2:
418 WT=69,29; Prm2$^{\Delta c/+}$=42,07; Prm2$^{\Delta c/-}$=26.78)(ANOVA: F(2)=18.98,p=0.009; Post-hoc Tukey

419 HSD: WT vs. Prm2$^{\Delta c/+}$: p=0.04, WT vs. Prm2$^{\Delta c/-}$: p=0.008). This does not seem to be the case
420 in Prm2$^{+/-}$ males, for which we find the percentage of PRM2 (including precursors) to be
421 similar to the wildtype (%PRM2=66.57 (n=1)) (Fig. 4D, Fig. S7). These data, together with
422 the mP2 signal detected in condensing spermatid cytoplasm (Fig. 2A), strongly suggest, that
423 loss of the cP2 domain leads to a reduction of PRM2 associated with DNA.
424
425 Histone-to-protamine transition is incomplete in Prm2$^{\Delta c/+}$ and Prm2$^{\Delta c/-}$ males
426 Since we found the relative level of PRM2 to be reduced, and PRM2 aberrantly located in the
427 cytoplasm and residual bodies of condensing/condensed spermatids in the testis, we next
428 evaluated the histone-to-protamine transition. To this end, we performed IHC staining to
429 detect histone H3, transition protein 1 (TNP1) and PRM1 in testis and epididymis sections. In
430 Prm2$^{\Delta c/+}$ male mice PRM1 staining intensity and localization is comparable to the WT.
431 However, PRM1 staining seems to be lost in Prm2$^{\Delta c/-}$ sperm from cauda epididymis (Fig. S6,
432 Fig. 5). This is most likely due to the strong degradation of the sperm and its DNA and low
433 sperm count in this genotype. We did not find any apparent increase in total histone H3
434 signal (Fig. S6, Fig. 5), However, in contrast to WT, TNP1 was retained in both Prm2$^{\Delta c/+}$ and
435 Prm2$^{\Delta c/-}$ males in step 15-16 spermatids and caput epididymal sperm. In cauda epididymal
436 sperm however, we did not find any visible signal of TNP1 (Fig. S6, Fig. 5). This indicates,
437 that loss of cP2 leads to transition protein retention.
438 In order to further investigate histone retention and alteration in nuclear protein content we
439 performed mass spectrometric analysis on mature sperm basic nuclear protein extracts and
440 analyzed differential abundance (DA) of the detected proteins. Compared to wildtype, we
441 found 14 proteins to be DA in Prm2$^{\Delta c/+}$ sperm, 20 in Prm2$^{\Delta c/-}$ males and 24 for Prm2$^{-/-}$ sperm.
442 Seven proteins were DA in all three comparisons, several of those associated with stress
443 response and/or apoptosis (HSPA2, B2M, CLU) (Fig. 6A,B). Consistent with IHC results we
444 did not find any histones that were significantly higher abundant in Prm2$^{\Delta c/+}$ or Prm2$^{\Delta c/-}$ males.
445 We therefore conclude that histone retention is not increased in males harboring the Prm2$^{\Delta c}$
446 allele. Interestingly in the Prm2$^{-/-}$ samples we did find histones (H3f3, H3C, H4C) to be

447 significantly higher abundant, indicating increased histone retention when PRM2 is
448 completely lacking. Transition proteins were not detected. Lists of DA proteins including
449 statistics can be found in supplementary dataset S2.
450 Eight proteins were not DA in Prm2$^{-/-}$ compared to WT, but in Prm2$^{\Delta c/+}$ and/or Prm2$^{\Delta c/-}$ males.
451 Of these, RPL26 and GSTM5 are involved in DNA damage response and/or oxidative stress
452 pathways, while TUBA3B and ANT4 (*Slc25a31*) are related to motility. Of note, citrate
453 synthase (CS) is specifically higher abundant in Prm2$^{\Delta c/+}$ and Prm2$^{\Delta c/-}$ males. Most
454 interestingly, we found the histone H2A variant H2A.L.2 to be significantly lower abundant in
455 Prm2$^{\Delta c/-}$ males, compared to the wildtype (Fig. 6A-D). H2A.L.2 is a spermatid/sperm-specific
456 histone variant and a key player in histone-to-protamine transition. Together with TH2B it
457 forms a nucleosome with an open chromatin structure allowing for loading of transition
458 proteins followed by protamine recruitment and histone and transition protein eviction by
459 protamines (Barral et al. 2017) (Fig. 6D). According to Hoghoughi et al. (2020) H2A.L.2 is
460 retained in mature sperm in pericentric heterochromatin. We therefore investigated the
461 presence and co-localization of H2A.L.2 and PRM2 in Prm2$^{\Delta c/-}$ and Prm2$^{\Delta c/+}$ males, by
462 immunofluorescent staining of condensed step 15-16 spermatids from tubule preparations
463 and mature sperm extracted from the cauda epididymis. In the wildtype, we found a
464 moderately strong signal for H2A.L.2 in the pericentric region of the nucleus, with PRM2
465 signal in the whole nucleus (Fig. 7a-b,g-h). However, in Prm2$^{\Delta c/+}$ and Prm2$^{\Delta c/-}$ step 15-16
466 spermatids the H2A.L.2 signal is stronger compared to the WT and localized in DAPI-bright
467 foci in the nucleus (Fig. 7c-f). DAPI-bright regions in nuclei usually correspond to
468 heterochromatin. In mature sperm, however, the H2A.L.2 signal is almost completely lost in
469 Prm2$^{\Delta c/+}$ and Prm2$^{\Delta c/-}$ males, consistent with the lower abundance found in mass
470 spectrometric analysis. The PRM2 signal is diffuse and distributed along the whole mature
471 sperm cell, likely due to severe membrane damage and degradation (Fig. 7i-l).
472
473 **Discussion**

474 The crucial role of protamines in the process of sperm chromatin reorganization is well
475 known. However, why two protamines are needed in some species, while PRM1 seems to be
476 sufficient in others is still unclear. The main difference between PRM1 and PRM2 is the
477 highly conserved N-terminal cleaved PRM2 domain (cP2). Its function remains elusive to
478 date. Using gene-editing we generated mice lacking the cleaved-*Prm2* (cP2) domain. We
479 show that the cP2 domain is indispensable for PRM2 function and required for male mouse
480 fertility. Mice heterozygous for the deletion of the domain display inviable and immotile
481 sperm. Loss of cP2 leads to severe retention of transition proteins and reduced incorporation
482 of PRM2 into nucleoprotamine. Instead, mature-PRM2 (mP2) is aberrantly found in
483 spermatid cytoplasm and residual bodies. While overall histone retention is not increased,
484 the histone variant H2A.L.2 is less abundant in mature sperm deficient in cP2.

485 Firstly, mP2 expressed from the $Prm2^{\Delta c}$ allele was detected in the nucleus of
486 condensed spermatids of cP2 deficient mice and was shown to be able to condense somatic
487 cell DNA *in-vitro* similar to PRM2, or PRM1 (Iuso et al. 2015). We therefore conclude that the
488 mP2 domain produced by gene editing seems to maintain its main function during
489 spermiogenesis in cP2 deficient mouse lines. Male $Prm2^{\Delta c/+}$ mice are infertile, show complete
490 fragmentation of mature sperm DNA, loss of viability and immotility of mature sperm. This is
491 in contrast to $PRM2^{+/-}$ males, which remained fertile (Schneider et al. 2016). In order to test,
492 whether the infertility of $Prm2^{\Delta c/+}$ mice is due to an aberrant interaction between mP2 and the
493 wildtype PRM2 precursor, we bred the $Prm2^{\Delta c}$ allele with the $Prm2^{\Delta 97bp}$ mouse line generated
494 and analyzed by Schneider et al. (2016, 2020). However, mice expressing only mP2
495 ($Prm2^{\Delta c/-}$) were also infertile showing an even more extreme phenotype than $Prm2^{\Delta c/+}$ males.
496 Since $Prm2^{+/-}$ male mice are reported to be fertile, these data clearly indicate, that loss of
497 cP2 leads to male infertility in mice. We speculate, that this holds also true for all other
498 species which harbor a functional PRM2 gene.

499 Since mature sperm chromatin is completely fragmented in cP2 deficient males and
500 mature sperm are inviable and immotile similar to $Prm2^{-/-}$ sperm, we suspected that sperm
501 might undergo epididymal degradation mediated by oxidative stress. Schneider et al. (2020)

502 showed that loss of PRM2 seems to lead to reduced antioxidant capacity of sperm, initiating
503 an oxidative stress-mediated destruction cascade during epididymal transit. Indeed, cP2
504 deficient mice showed a strong increase in oxidative DNA damage in the cauda epididymis.
505 Prm2$^{\Delta c/-}$ sperm seem to be degraded to an extent that many of the caudal sperm are
506 completely disintegrated, leading to a significantly reduced sperm count. We propose that
507 this is not a specific effect of cP2 or PRM2 deficiency but an inherent epididymal mechanism
508 evoked by DNA damage or aberrant protamination (or even otherwise damaged sperm, e.g.:
509 membrane defects, aberrant morphology or sperm surface proteome). How sperm damage
510 might be sensed by epididymal cells and what, in fact, initiates this cascade is an interesting
511 avenue for further investigation.

512 Given the timing of *Prm2* expression and processing, the primary effects of cP2 loss
513 are likely to be found during the transition from histone-bound to protaminized DNA in the
514 final stages of spermiogenesis. Barral et al. (2017) describe this transition taking place by
515 assembly of a histone (TH2B and H2A.L.2) - transition protein (TNP1 and TNP2) interface
516 followed by protamine recruitment and processing. Protamines themselves subsequently
517 replace histones. This process is disrupted in cP2 deficient mice.

518 Firstly, in cP2 deficient mice mP2 is detected in the cytoplasm and residual bodies in
519 addition to the signal found in the nucleus, indicating that mP2 is not completely incorporated
520 into the condensing chromatin. In consequence, the protamine ratio changes from 2:1 in
521 wildtype to 1:2-1:5 in cP2 deficient sperm. This indicates, that the cP2 domain facilitates
522 incorporation of PRM2 and assembly of nucleoprotamine.

523 Secondly, we found retention of TNP1 in condensed testicular spermatids and caput
524 epididymal sperm, indicating that the eviction of TNP1 is hampered due to the loss of cP2 or
525 that TNP1 is binding DNA in a competitive manner. Of note, a recent study investigating a
526 single residue mutation in PRM1 showed increased histone retention, but no disturbances in
527 transition protein retention in such mice (Moritz et al. 2021). Transition proteins are believed
528 to aid in chromatin condensation by stabilizing the DNA in a non-supercoiled state,
529 cooperating with topoisomerases to relieve torsional stress and to be involved in DNA repair

530 during chromatin condensation (Singh and Rao, 1988 Lèvesque et al. 1998, Akama et al.
531 1999). Loss of either transition protein results in incomplete PRM2 processing (Yu et al.
532 2000, Shirley et al. 2004, Zhao et al. 2004) and TNP2 was shown to interact with PRM2
533 (Barral et al. 2017). This demonstrates that transition proteins are required for proper PRM2
534 processing during nucleoprotamine assembly. The fact that we find severe retention of TNP1
535 in condensed spermatids indicates, that the cP2 domain in turn, is required for the proper
536 processing (i.e. eviction) of TNP1.

537 Surprisingly, however, overall histone retention was not increased. This was
538 confirmed by H3 immunostaining and mature sperm basic nuclear protein abundance
539 analysis. Interestingly, we do find an increased retention of H3 and H4 variants in Prm2$^{-/-}$
540 deficient sperm. The data from the H3 immunostainig indicate, that the global amount of
541 retained histones seems unaffected, and hence not controlled by protamine ratio or PRM2
542 processing.

543 The retention of transition protein detected in cP2 deficient mice seems to go along
544 with altered retention of H2A.L.2. During the first steps of chromatin condensation H2A.L.2,
545 together with TH2B provides an open chromatin interface necessary for transition protein
546 loading. Barral et al. (2017) showed, that deletion of H2A.L.2 leads to infertility, aberrant
547 transition protein loading and disturbed processing of PRM2. In mature sperm H2A.L.2 was
548 shown to be retained in pericentric heterochromatin (Govin et al. 2007, Hoghoughi et al.
549 2020). This retention seems to be lost in Prm2$^{\Delta c/-}$ mature sperm, where H2A.L.2 was shown
550 to be significantly lower abundant. However, a strong H2A.L.2 signal can be observed in
551 Prm2$^{\Delta c/-}$ condensed spermatids in the testis, were it overlaps with atypical speckles of bright
552 DAPI signal. Thus, it seems that H2A.L.2-transition protein complexes are retained in
553 aberrant clumps of heterochromatin in cP2 deficient mice.

554 Protamines have a strong electrostatic attraction to DNA due to arginine clusters
555 (Moritz et al. 2021). This allows protamines to condense DNA even in the absence of
556 spermatid specific histones and transition proteins, as shown in *in-vitro* assays in somatic
557 cells and in this study (Iuso et al. 2015). However, uncontrolled or unbalanced binding of

558 protamines might lead to strong torsional stress and DNA damage. A controlled stepwise
559 chromatin condensation therefore could be required to maintain chromatin integrity. Moritz et
560 al. (2021) recently showed that the PRM2 precursor has a lower DNA binding affinity than
561 mP2, leading to faster DNA condensation by mP2. Barral et al. (2017) suggested that
562 transition proteins buffer protamine incorporation by allowing for ordered protamine loading
563 and (or possibly through) PRM2 processing. By losing the cP2 domain this processing step is
564 skipped. We therefore propose, that the aberrant interaction with transition proteins due to
565 cP2 deficiency leads to random mP2 binding, leading to strong hypercondensation of open
566 chromatin resulting in DNA strand breaks. Transition protein-loaded chromatin, however
567 does not allow for mP2 loading, leading to incomplete mP2 incorporation and retention of
568 H2A.L.2 – transition protein complexes in aberrantly located heterochromatin foci, that are
569 lost by DNA degradation during epididymal transit.
570 In conclusion, our results show that the cleaved domain of PRM2 is essential for
571 sperm function and fertility. Loss of the domain leads to incomplete protamination, a switch in
572 the protamine ratio and transition protein retention in epididymal sperm. During epididymal
573 transit cP2 deficient sperm are degraded, seemingly by ROS mediated damage, leading to
574 complete DNA fragmentation. cP2 seems to be necessary for correct interaction between the
575 H2A.L.2 - transition protein complex and PRM2. We were able to provide a first glimpse into
576 the function of cleaved PRM2 and PRM2 processing, that opens up multiple avenues for
577 further investigation.
578
579 **Acknowledgments:** This study was supported by grants from the Deutsche
580 Forschungsgemeinschaft (DFG) to L.A. (AR 1221/1-1) and H.S. (Scho 503/15-2). L.A. was
581 further supported by the University of Bonn Medical school supplementary research grant
582 program *FEMHABIL.* We thank Gaby Beine, Angela Egert and Andrea Jäger for excellent
583 technical assistance. Protein identifications were done at the Core Facility Mass
584 Spectrometry, Institute of Biochemistry and Molecular Biology, Medical Faculty, University of
585 Bonn. Mass spectrometer funded by the Deutsche Forschungsgemeinschaft (DFG) –

586 Projektnummer 386936527. RNAseq was done at University of Bonn Core facility for Next
587 Generation Sequencing (NGS). We thank Saadi Khochbin and Sophie Barral for the gift of
588 the H2A.L.2 antibody and excellent advice.
589
590 **Author contributions:** L.A. and H.S. conceived the study and designed the experiments.
591 L.A. and S.S. generated gene-edited mice. L.A. and G.E.M. analysed gene-edited mice.
592 F.E.O. and I.N. generated IHC stainings. L.A. and H.S. drafted the manuscript. All authors
593 read and approved the final manuscript.
594
595 **References**

596 Ahlmann-Eltze C, Anders S. proDA: Probabilistic dropout analysis for identifying differentially
597 abundant proteins in label-free mass spectrometry. Biorxiv. 2020; 1:661496.
598 Akama K, Kondo M, Sato H, Nakano M. Transition protein 4 from boar late spermatid nuclei
599 is a topological factor that stimulates DNA-relaxing activity of topoisomerase I. FEBS
600 letters. 1999; 442:189-92.
601 Aoki VW, Liu L, Jones KP, Hatasaka HH, Gibson M, Peterson CM, Carrell DT. Sperm
602 protamine 1/protamine 2 ratios are related to in vitro fertilization pregnancy rates and
603 predictive of fertilization ability. Fertility and Sterility. 2006; 86:1408-15.
604 Balhorn R. Mammalian Proteins: structure and Molecular Interaction. In: Adolph KW, editor.
605 Molecular Biology of Chromosome Function. New York: Springer Verlag; 1989. pp. 366–
606 395.
607 Balhorn R. The protamine family of sperm nuclear proteins. Genome Biol. 2007; 227.
608 doi:10.1186/gb-2007-8-9-227
609 Barral S, Morozumi Y, Tanaka H, Montellier E, Govin J, de Dieuleveult M, et al. Histone
610 Variant H2A.L.2 Guides Transition Protein-Dependent Protamine Assembly in Male Germ
611 Cells. Mol Cell. 2017; 89–101.e8. doi:10.1016/j.molcel.2017.02.025

612 Chauviere M, Martinge A, DeBarle M, Sautiere P, Chevallier P. Molecular characterization of
613 six intermediate proteins in the processing of mouse protamine P2 precursor. Eur J
614 Biochem. 1992; 759–765. doi:10.1111/j.1432-1033.1992.tb16691.x
615 Chen H, Cheung MPL, Chow PH, Cheung ALM, Liu W, O WS. Protection of sperm DNA
616 against oxidative stress in vivo by accessory sex gland secretions in male hamsters.
617 Reproduction. 2002; 491–499.
618 Corzett M, Mazrimas J, Balhorn R. Protamine 1: Protamine 2 stoichiometry in the sperm of
619 eutherian mammals. Mol Reprod Dev. 2002; 519–527. doi:10.1002/mrd.10105
620 de Mateo S, Gázquez C, Guimerà M, Balasch J, Meistrich ML, Ballescà JL, Oliva R.
621 Protamine 2 precursors (Pre-P2), protamine 1 to protamine 2 ratio (P1/P2), and assisted
622 reproduction outcome. Fertility and sterility. 2009; 91:715-22.
623 de Mateo S, Ramos L, de Boer P, Meistrich M, Oliva R. Protamine 2 precursors and
624 processing. Protein and peptide letters. 2011; 18:778-85.
625 de Yebra L, Ballescá JL, Vanrell JA, Corzett M, Balhorn R, Oliva R. Detection of P2
626 precursors in the sperm cells of infertile patients who have reduced protamine P2 levels.
627 Fertil Steril. 1998; 755–9.
628 García-Peiró A, Martínez-Heredia J, Oliver-Bonet M, Abad C, Amengual MJ, Navarro J,
629 Jones C, Coward K, Gosálvez J, Benet J. Protamine 1 to protamine 2 ratio correlates with
630 dynamic aspects of DNA fragmentation in human sperm. Fertility and sterility. 2011;
631 95:105-9.
632 Govin J, Escoffier E, Rousseaux S, Kuhn L, Ferro M, Thévenon J, Catena R, Davidson I,
633 Garin J, Khochbin S, Caron C. Pericentric heterochromatin reprogramming by new
634 histone variants during mouse spermiogenesis. The Journal of cell biology. 2007;
635 176:283-94.
636 Hada M, Masuda K, Yamaguchi K, Shirahige K, Okada Y. Identification of a variant-specific
637 phosphorylation of TH2A during spermiogenesis. Sci Rep. 2017; 46228.
638 doi:10.1038/srep46228

639 Hoghoughi N, Barral S, Curtet S, Chuffart F, Charbonnier G, Puthier D, Buchou T,
640 Rousseaux S, Khochbin S. RNA-Guided genomic localization of H2A. L. 2 histone variant.
641 Cells. 2020; 9:474.
642 Ishibashi T, Li A, Eirín-López JM, Zhao M, Missiaen K, Abbott DW, Meistrich M, Hendzel MJ,
643 Ausio J. H2A. Bbd: an X-chromosome-encoded histone involved in mammalian
644 spermiogenesis. Nucleic acids research. 2010; 38:1780-9.
645 Iuso D, Czernik M, Toschi P, Fidanza A, Zacchini F, Feil R, Curtet S, Buchou T, Shiota H,
646 Khochbin S, Ptak GE. Exogenous expression of human protamine 1 (hPrm1) remodels
647 fibroblast nuclei into spermatid-like structures. Cell reports. 2015; 13:1765-71.
648 Käll L, Storey JD, MacCoss MJ, Noble WS. Assigning significance to peptides identified by
649 tandem mass spectrometry using decoy databases. Journal of proteome research. 2008;
650 7:29-34.
651 Kim D, Langmead B, Salzberg S L. HISAT: A fast spliced aligner with low memory
652 requirements. Nat Methods. 2015; 12:357–360.
653 Kotaja N, Kimmins S, Brancorsini S, Hentsch D, Vonesch JL, Davidson I, Parvinen M,
654 Sassone-Corsi P. Preparation, isolation and characterization of stage-specific
655 spermatogenic cells for cellular and molecular analysis. Nature methods. 2004;1:249-54.
656 Krawetz SA, Dixon GH. Sequence similarities of the protamine genes: Implications for
657 regulation and evolution. J Mol Evol. 1988; 291–297. doi:10.1007/BF02101190
658 Lévesque D, Veilleux S, Caron N, Boissonneault G. Architectural DNA-binding properties of
659 the spermatidal transition proteins 1 and 2. Biochemical and biophysical research
660 communications. 1998; 252:602-9.
661 Love M I, Huber W, Anders S. 2014. Moderated estimation of fold change and dispersion for
662 RNA-seq data with DESeq2. Genome Biol. 2014; 15:1–21.
663 Lüke L, Campbell P, Varea Sánchez M, Nachman MW, Roldan ERS. Sexual selection on
664 protamine and transition nuclear protein expression in mouse species. Proc Biol Sci.
665 2014; 20133359. doi:10.1098/rspb.2013.3359

666 Lüke L, Tourmente M, Roldan ERS. Sexual selection of protamine 1 in mammals. Mol Biol
667 Evol. 2016; 174–184. doi:10.1093/molbev/msv209
668 Lüke L, Vicens A, Serra F, Luque-Larena JJ, Dopazo H, Roldan ERS, et al. Sexual Selection
669 Halts the Relaxation of Protamine 2 among Rodents. PLoS One. 2011; e29247.
670 doi:10.1371/journal.pone.0029247
671 Lüke L, Vicens A, Tourmente M, Roldan ERS. Evolution of protamine genes and changes in
672 sperm head phenotype in rodents. Biol Reprod. 2014; 67.
673 doi:10.1095/biolreprod.113.115956
674 Mellacheruvu D, Wright Z, Couzens AL, Lambert JP, St-Denis NA, Li T, Miteva YV, Hauri S,
675 Sardiu ME, Low TY, Halim VA. The CRAPome: a contaminant repository for affinity
676 purification–mass spectrometry data. Nature methods. 2013; 10:730-6.
677 Mi H, Huang X, Muruganujan A, Tang H, Mills C, Kang D, Thomas PD. 2017. PANTHER
678 version 11: Expanded annotation data from Gene Ontology and Reactome pathways, and
679 data analysis tool enhancements. Nucleic Acids Res. 2017; 45:D183–D189.
680 Moritz L, Schon S, Rabbani M, Sheng Y, Pendlebury D, Agrawal R, Sultan C, Jorgensen K,
681 Zheng X, Diehl A, Ragunathan K. Single residue substitution in protamine 1 disrupts
682 sperm genome packaging and embryonic development in mice. bioRxiv. 2021.
683 Oliva R, Dixon GH. Vertebrate protamine genes and the histone-to-protamine replacement
684 reaction. Biology WEC and KMBT-P in NAR and M, editor. Prog Nucleic Acid Res Mol
685 Biol; 1991; 25–94.
686 Pertea M, Pertea GM, Antonescu CM, Chang TC, Mendell JT, Salzberg SL. 2015. StringTie
687 enables improved reconstruction of a transcriptome from RNA-seq reads. Nat Biotechnol.
688 2015; 33:290–295.
689 Piunti A, Shilatifard A. The roles of Polycomb repressive complexes in mammalian
690 development and cancer. Nature Reviews Molecular Cell Biology. 2021; 22:326-45.
691 Rathke C, Baarends WM, Awe S, Renkawitz-Pohl R. Chromatin dynamics during
692 spermiogenesis. Biochimica et Biophysica Acta - Gene Regulatory Mechanisms. 2014;
693 155–168. doi:10.1016/j.bbagrm.2013.08.004

694 Retief JD, Dixon GH. Evolution of pro-protamine P2 genes in primates. Eur J Biochem. 1993;
695 609–615. doi:10.1111/j.1432-1033.1993.tb17960.x
696 Retief JD, Winkfein RJ, Dixon GH, Adroer R, Queralt R, Ballabriga J, et al. Evolution of
697 Protamine P1 Genes in Primates. J Mol Evol. 1993; 426–434.
698 Robinson JT, Thorvaldsdóttir H, Winckler W, Guttman M, Lander ES, Getz G, Mesirov JP.
699 Integrative genomics viewer. Nature biotechnology. 2011; 29:24-6.
700 Ruiz-Lopez MJ, Espeso G, Evenson DP, Roldan ERS, Gomendio M. Paternal levels of DNA
701 damage in spermatozoa and maternal parity influence offspring mortality in an
702 endangered ungulate. Proc R Soc B Biol Sci. 2010; 2541–2546.
703 doi:10.1098/rspb.2010.0333
704 Schneider S, Shakeri F, Trötschel C, Arévalo L, Kruse A, Buness A, Poetsch A, Steger K,
705 Schorle H. Protamine-2 deficiency initiates a reactive oxygen species (ROS)-mediated
706 destruction cascade during epididymal sperm maturation in mice. Cells. 2020; 9:1789.
707 Schneider S, Balbach M, Jan F. Jikeli, Fietz D, Nettersheim D, Jostes S, et al. Re-visiting the
708 Protamine-2 locus: deletion, but not haploinsufficiency, renders male mice infertile. Sci
709 Rep. 2016; 36764. doi:10.1038/srep36764
710 Shirley CR, Hayashi S, Mounsey S, Yanagimachi R, Meistrich ML. Abnormalities and
711 reduced reproductive potential of sperm from Tnp1-and Tnp2-null double mutant mice.
712 Biology of reproduction. 2004;71:1220-9.
713 Singh J, Rao MRS. Interaction of rat testis protein, TP, with nucleosome core particle.
714 Biochem Int. 1988; 17:701–710
715 Skinner BM, Rathje CC, Bacon J, Johnson EE, Larson EL, Kopania EE, Good JM, Yousafzai
716 G, Affara NA, Ellis PJ. A high-throughput method for unbiased quantitation and
717 categorization of nuclear morphology. Biology of reproduction. 2019; 100:1250-60.
718 Soler-Ventura A, Castillo J, de la Iglesia A, Jodar M, Barrachina F, Ballesca JL, Oliva R.
719 Mammalian sperm protamine extraction and analysis: a step-by-step detailed protocol and
720 brief review of protamine alterations. Protein and peptide letters. 2018; 25:424-33.

721 Steger K, Wilhelm J, Konrad L, Stalf T, Greb R, Diemer T, Kliesch S, Bergmann M, Weidner
722 W. Both protamine-1 to protamine-2 mRNA ratio and Bcl2 mRNA content in testicular
723 spermatids and ejaculated spermatozoa discriminate between fertile and infertile men.
724 Human Reproduction. 2008; 23:11-6.
725 Tanaka H, Baba T. Gene expression in spermiogenesis. Cell Mol Life Sci. 2005; 344–354.
726 doi:10.1007/s00018-004-4394-y
727 Torregrosa N, Domínguez-Fandos D, Camejo MI, Shirley CR, Meistrich ML, Ballescà JL, et
728 al. Protamine 2 precursors, protamine 1/protamine 2 ratio, DNA integrity and other sperm
729 parameters in infertile patients. Hum Reprod. 2006; 2084–9. doi:10.1093/humrep/del114
730 Tourmente M, Gomendio M, Roldan ERS. Sperm competition and the evolution of sperm
731 design in mammals. BMC Evol Biol. 2011; 12. doi:10.1186/1471-2148-11-12
732 Wickham H. ggplot2. Wiley Interdisciplinary Reviews: Computational Statistics. 2011; 3:180-
733 5.
734 Yelick P, Balhorn ROD, Johnson PA, Corzett M, Mazrimas JOEA, Kleene KKC, et al. Mouse
735 protamine 2 is synthesized as a precursor whereas mouse protamine 1 is not. Mol Cell
736 Biol. Am Soc Microbiol; 1987; 2173. doi:10.1128/MCB.7.6.2173.
737 Yu YE, Zhang Y, Unni E, Shirley CR, Deng JM, Russell LD, Weil MM, Behringer RR,
738 Meistrich ML. Abnormal spermatogenesis and reduced fertility in transition nuclear protein
739 1-deficient mice. Proceedings of the National Academy of Sciences. 2000; 97:4683-8.
740 Zatecka E, Castillo J, Elzeinova F, Kubatova A, Ded L, Peknicova J, Oliva R. The effect of
741 tetrabromobisphenol A on protamine content and DNA integrity in mouse spermatozoa.
742 Andrology. 2014; 2:910-7.
743 Zhao M, Shirley CRCR, Yu YEE, Mohapatra B, Zhang YUN, Unni E, et al. Targeted
744 disruption of the transition protein 2 gene affects sperm chromatin structure and reduces
745 fertility in mice. Mol Cell Biol. 2001; 7243. doi:10.1128/MCB.21.21.7243
746 Zhao M, Shirley CR, Mounsey S, Meistrich ML. Nucleoprotein transitions during
747 spermiogenesis in mice with transition nuclear protein Tnp1 and Tnp2 mutations. Biology
748 of reproduction. 2004; 71:1016-25.

749

750 **Figure legends**

751 **Figure 1.** Gene editing, fertility and expression. A) Schematic representation of the
752 generation of cP2 deletion. Double strand breaks induced by Cas9 indicated by black
753 triangles. B) Schematic overview of analyzed genotypes and fertility. $Prm2^{+/-}$ and $Prm2^{-/-}$
754 (Schneider et al. 2016) were included as a comparison. Barplot of average litter size for WT,
755 $Prm2^{+/-}$, $Prm2^{-/-}$, $Prm2^{\Delta c/+}$ and $Prm2^{\Delta c/-}$, n=5 for each genotype. C) Barplot showing average
756 DESeq2 normalized read counts of *Prm2* for WT, $Prm2^{\Delta c/+}$ and $Prm2^{\Delta c/-}$. D) Barplot showing
757 comparison between number of differentially higher and lower expressed genes for $Prm2^{\Delta c/+}$
758 and $Prm2^{\Delta c/-}$ compared to wildtype.

759

760 **Figure 2.** Localization and DNA condensing ability of mP2. A) Immunohistochemical
761 fluorescent staining of PRM2 (WT, $Prm2^{\Delta c/+}$) or mP2 ($Prm2^{\Delta c/+}$, $Prm2^{\Delta c/-}$) (green) in testis
762 sections, counterstaining with DAPI (blue). Scale bar = 50µm. B) Heterologous expression of
763 plasmids encoding eGFP tagged PRM2 (*Prm2*-eGFP) or mP2 (*mP2*-eGFP) in human
764 embryonic kidney 293 (HEK) cells 48 hours post-transfection. Scale bar = 10µm.

765

766 **Figure 3.** Sperm and testis parameters and histology. A) Barplots showing data for relative
767 testes mass, mature sperm count, percentage of viable mature sperm (eosin-nigrosin assay)
768 and percentage of motile mature sperm in $Prm2^{\Delta c/+}$ and $Prm2^{\Delta c/-}$ mice compared to wildtype.
769 B) PAS staining of testis and epididymal sections of $Prm2^{\Delta c/+}$, $Prm2^{\Delta c/-}$ and WT males. Scale
770 bar = 50µm (200µm for left column).

771

772 **Figure 4.** Chromatin integrity, nuclear morphology and protamine content. A) Agarose gel of
773 DNA extracted from WT, $Prm2^{+/-}$, $Prm2^{-/-}$ and $Prm2^{\Delta c/+}$ mature sperm. B)
774 Immunohistochemical fluorescent staining of 8-Oxo-2'-deoxyguanosine (8-OHdG) (green) in
775 caput epididymis (upper row) and cauda epididymis (lower row) of $Prm2^{\Delta c/+}$, $Prm2^{\Delta c/-}$ and WT.
776 Counterstained with DAPI (pseudo-colored grey). Scale bar = 50µm. C) Comparison of

777 mature sperm nucleus consensus shapes of WT, Prm2$^{+/-}$, Prm2$^{-/-}$, Prm2$^{\Delta c/+}$ and Prm2$^{\Delta c/-}$
778 resulting from nuclear morphology analysis. Numbers inside the consensus shapes indicate
779 the number of nuclei assessed and assigned to the respective consensus shape cluster.
780 Upper row shows the consensus shape of the different gene edited lines overlaid with the
781 wildtype consensus shape. cl. = cluster. D) Representative lanes of acid-urea gel
782 electrophoresis (AU-PAGE) of WT, Prm2$^{+/-}$, Prm2$^{-/-}$, Prm2$^{\Delta c/+}$ and Prm2$^{\Delta c/-}$ mature sperm
783 basic nuclear protein extractions. a=non-protamine basic nuclear proteins, b=PRM2
784 precursors, open arrowhead indicates mature PRM2 band, solid arrowhead indicates PRM1
785 band. To the right: quantification of the percentage of PRM2 (including PRM2 precursors) of
786 total protamine by band density analysis. Asterisk indicates significant difference.
787
788 **Figure 5.** Histone H3, transition protein 1 and protamine 1 staining. Two left columns:
789 Immunohistochemical fluorescent staining of Histone H3 (H3) (red) and protamine 1 (PRM1)
790 (green) in WT, Prm2$^{\Delta/+}$ and Prm2$^{\Delta/-}$ caput epididymis. Counterstained with DAPI (blue). Scale
791 bar = 50µm. Columns to the right: Immunohistochemical fluorescent staining of transition
792 protein 1 (TNP1) (red) and protamine 1 (PRM1) (green) in WT, Prm2$^{\Delta/+}$ and Prm2$^{\Delta/-}$ caput
793 and cauda epididymis. Counterstained with DAPI (blue). Scale bar = 50µm.
794
795 **Figure 6.** Differential abundance of mature sperm basic nuclear proteins. A) volcano plots
796 showing differential abundance (DA) of basic nuclear proteins in Prm2$^{\Delta/+}$ compared to WT
797 (upper plot) and Prm2$^{\Delta/-}$ compared to WT (lower plot). Significantly DA proteins are indicated
798 in color (teal = lower abundant, yellow = higher abundant). Top DA proteins and proteins of
799 interest are labeled with their corresponding gene symbol. B) Venn diagram showing the
800 overlap between DA proteins found in the three different comparisons (WT vs. Prm2$^{\Delta/+}$, WT
801 vs. Prm2$^{\Delta/-}$ and WT vs. Prm2$^{-/-}$). Proteins present in overlaps of interest are listed with their
802 corresponding gene symbol. H2A.L.2 is marked in red. C) Boxplot of median normalized log2
803 abundance of H2A.L.2 in WT, Prm2$^{-/-}$, Prm2$^{\Delta/+}$ and Prm2$^{\Delta/-}$. D) Interaction network for
804 H2A.L.2 extracted from String database (Szklarczyk et al. 2019).

805

806 **Figure 7.** Immunohistochemical staining of H2A.L.2 and PRM2. Immunohistochemical

807 fluorescent staining of H2A.L.2 (red) and PRM2 (green) in WT, $Prm2^{\Delta/+}$ and $Prm2^{\Delta/-}$ step 15-

808 16 spermatids from tubule preparations (two left columns) and mature sperm extracted from

809 cauda epididymis (two right columns). Counterstained with DAPI (blue). Scale bar = 20μm.

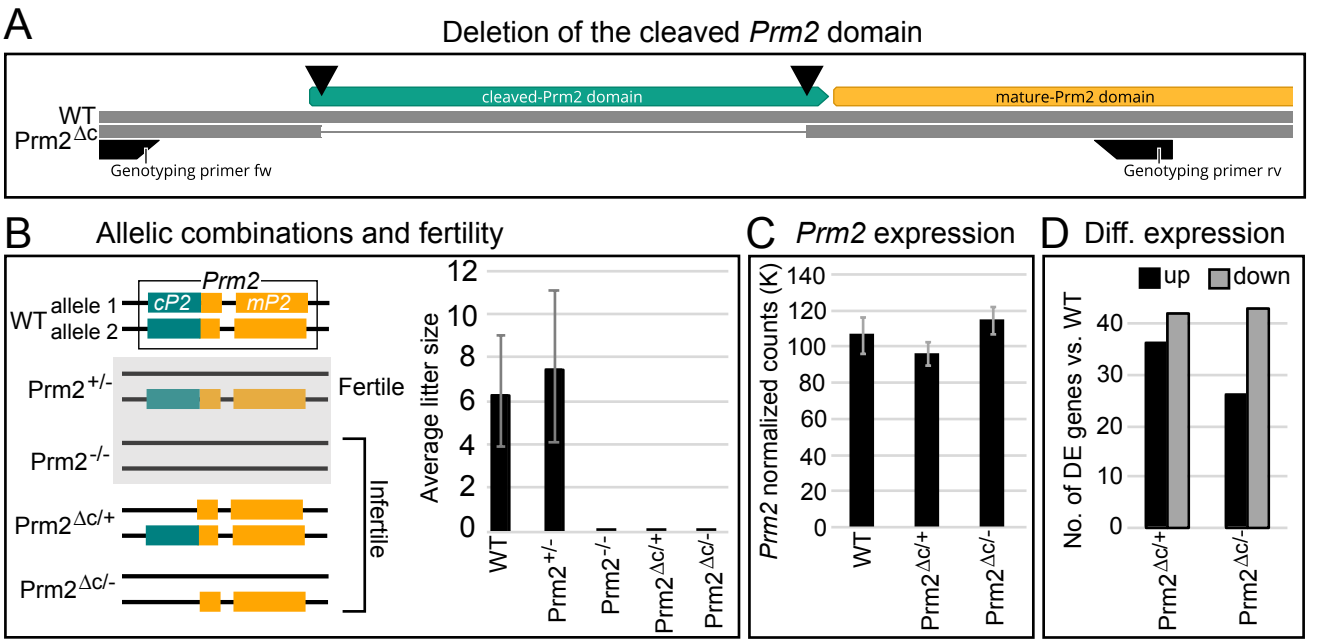
A
Deletion of the cleaved Prm2 domain
cleaved-Prm2 domain
mature-Prm2 domain
WT
Prm2Δc
Genotyping primer fw
Genotyping primer rv
B
Allelic combinations and fertility
Prm2
WT allele 1
allele 2
cP2
mP2
Prm2+/-
Fertile
Prm2-/-
Prm2Δc/+
Prm2Δc/-
Infertile
Average litter size
12
10
8
6
4
2
0
WT
Prm2+/-
Prm2-/-
Prm2Δc/+
Prm2Δc/-
C
Prm2 expression
Prm2 normalized counts (K)
140
120
100
80
60
40
20
0
WT
Prm2Δc/+
Prm2Δc/-
D
Diff. expression
up
down
No. of DE genes vs. WT
40
30
20
10
0
Prm2Δc/+
Prm2Δc/-

Fig. 1

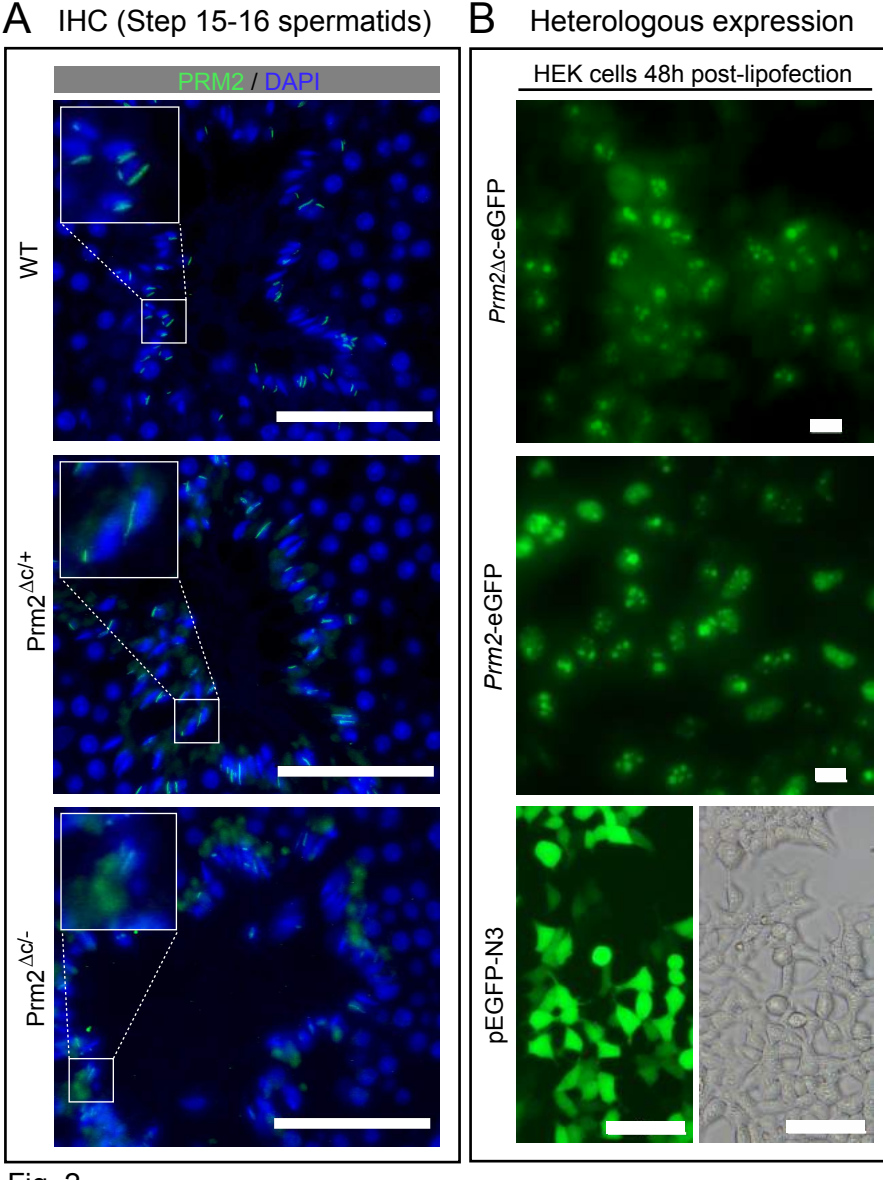
A
IHC (Step 15-16 spermatids)
PRM2 / DAPI
WT
Prm2Δc/+
Prm2Δc/-
B
Heterologous expression
HEK cells 48h post-lipofection
Prm2Δc-eGFP
Prm2-eGFP
pEGFP-N3

Fig. 2

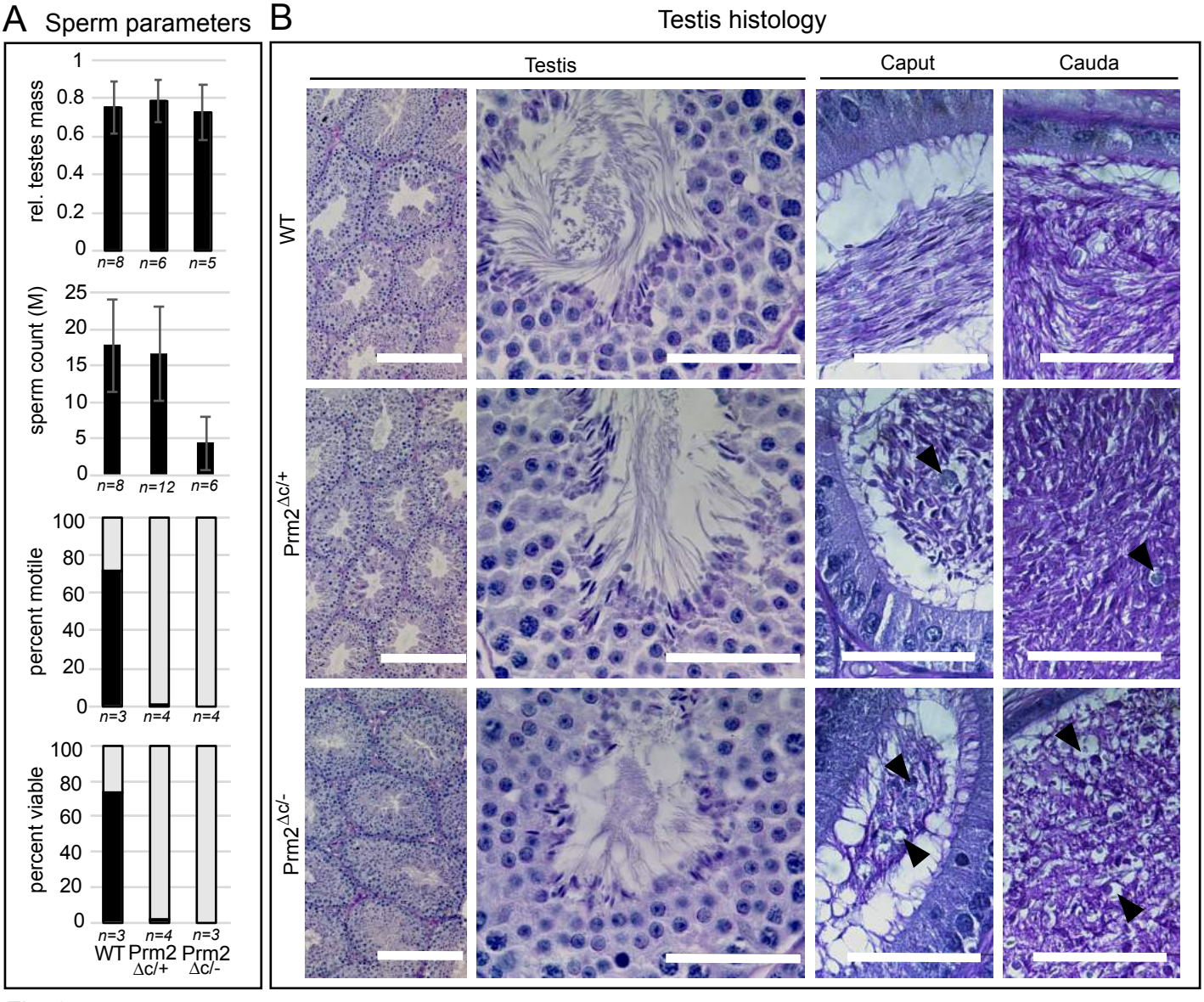
A
Sperm parameters
rel. testes mass
1
0.8
0.6
0.4
0.2
0
n=8
n=6
n=5
sperm count (M)
25
20
15
10
5
0
n=8
n=12
n=6
percent motile
100
80
60
40
20
0
n=3
n=4
n=4
percent viable
100
80
60
40
20
0
n=3
n=4
n=3
WT
Prm2 Δc/+
Prm2 Δc/-
B
Testis histology
Testis
Caput
Cauda
WT
Prm2Δc/+
Prm2Δc/-

Fig. 3

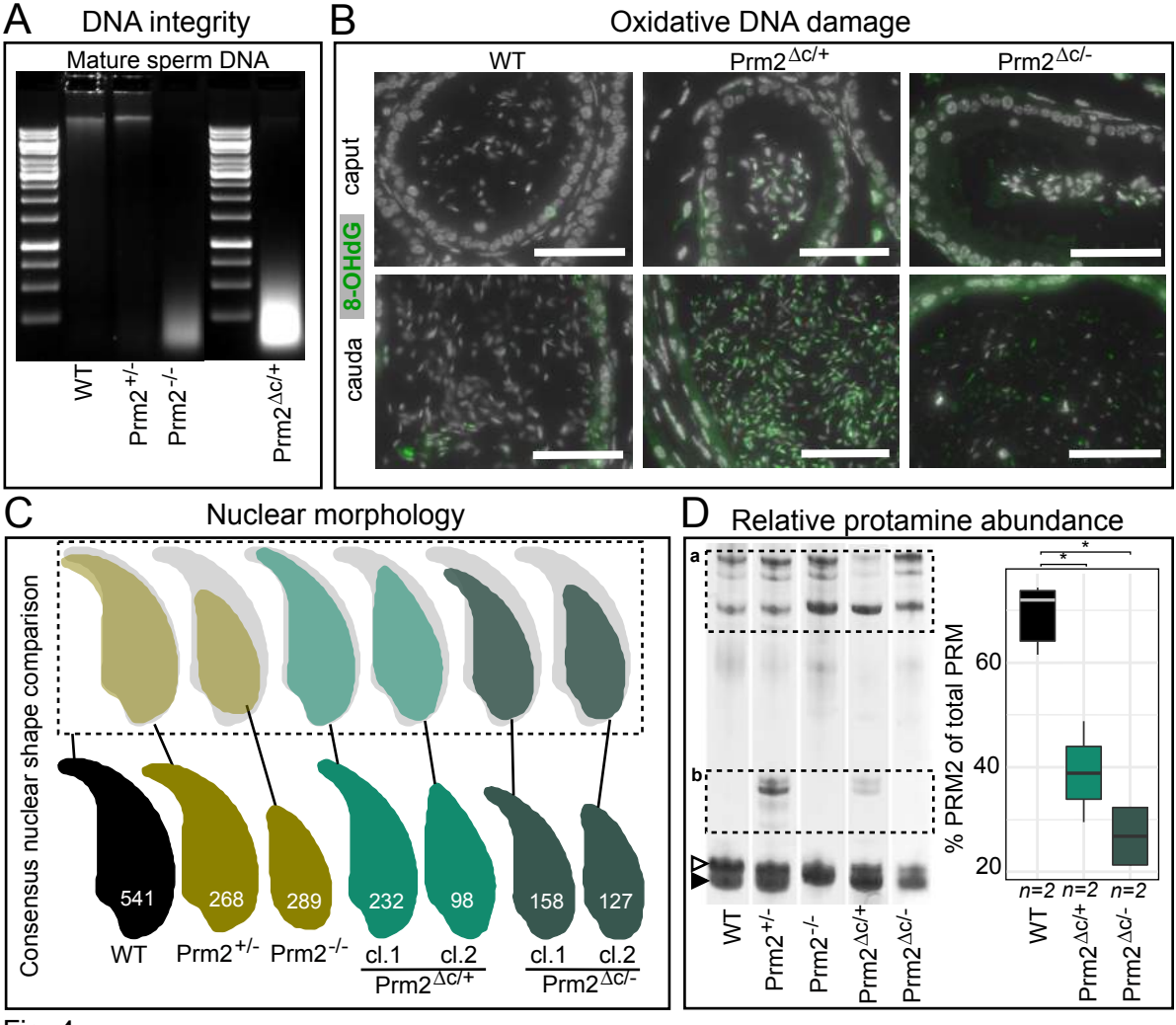
A
DNA integrity
Mature sperm DNA
WT
Prm2+/-
Prm2-/-
Prm2Δc/+
B
Oxidative DNA damage
WT
Prm2Δc/+
Prm2Δc/-
caput
8-OHdG
cauda
C
Nuclear morphology
Consensus nuclear shape comparison
541
268
289
232
98
158
127
WT
Prm2+/-
Prm2-/-
cl.1
cl.2
Prm2Δc/+
cl.1
cl.2
Prm2Δc/-
D
Relative protamine abundance
a
b
WT
Prm2+/-
Prm2-/-
Prm2Δc/+
Prm2Δc/-
% PRM2 of total PRM
60
40
20
n=2
n=2
n=2
WT
Prm2Δc/+
Prm2Δc/-

Fig. 4

Histone H3, Transition protein 1 and Protamine 1 IHC

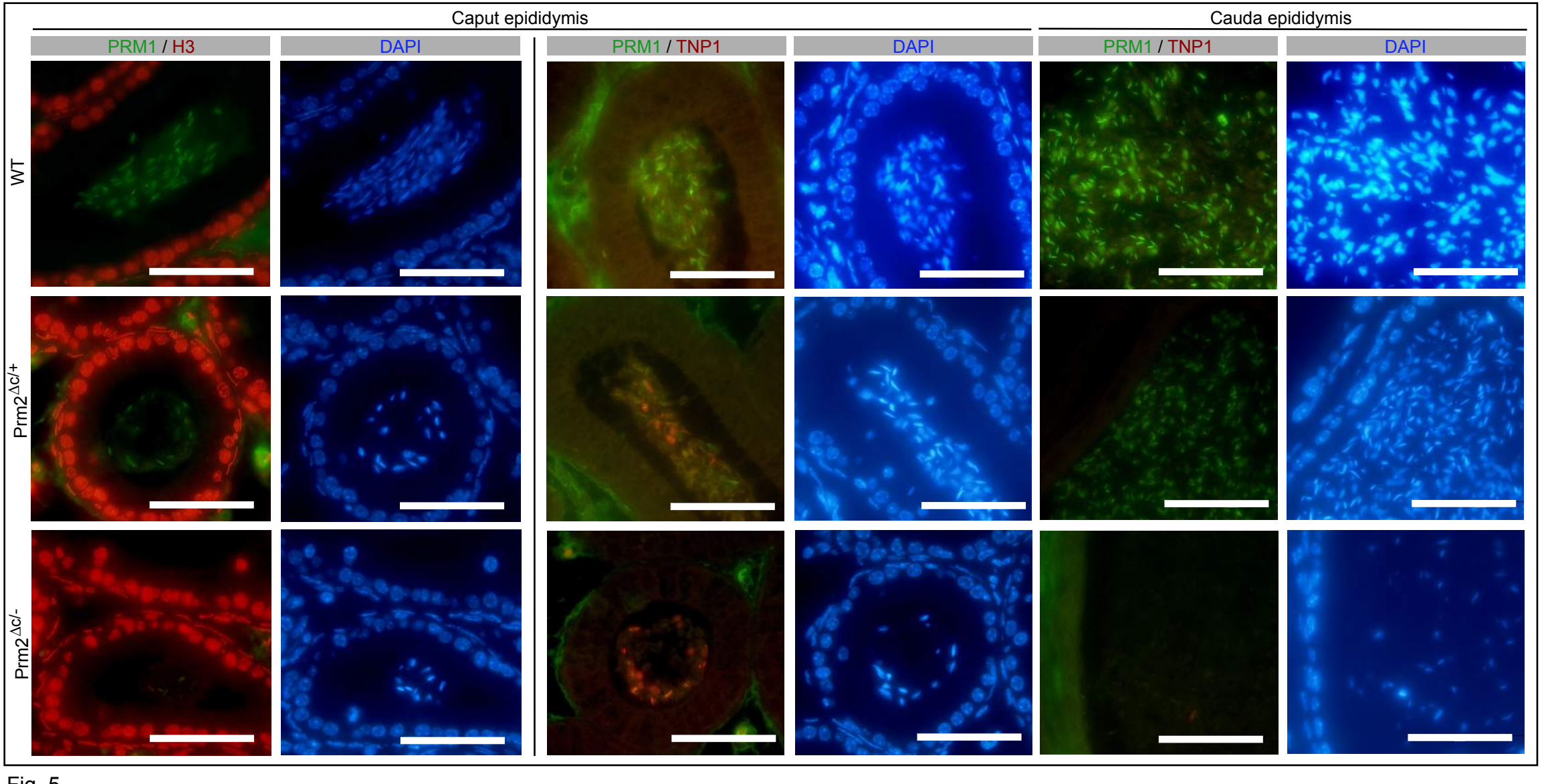

Fig. 5

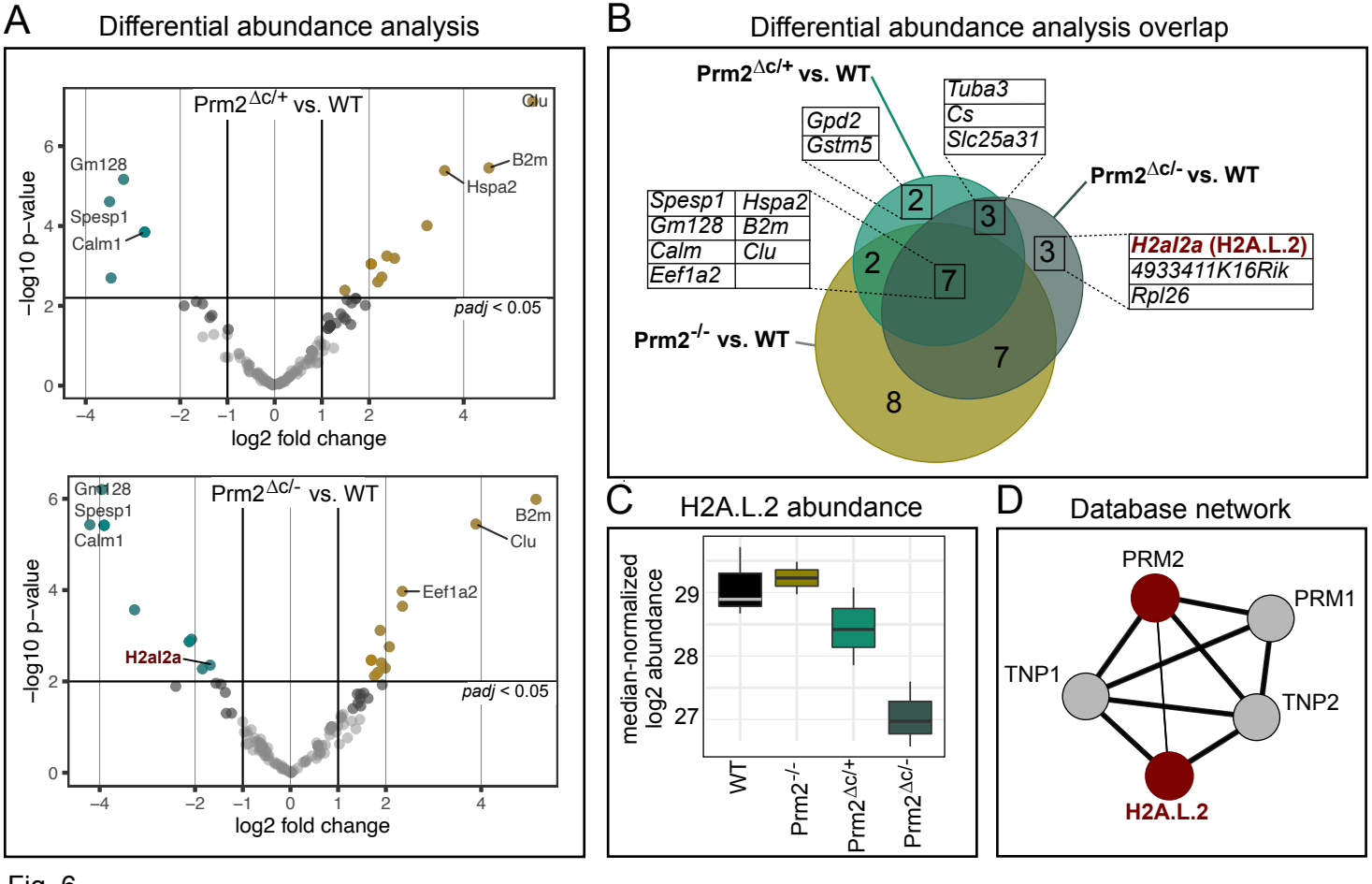
A
Differential abundance analysis
Prm2Δc/+ vs. WT
Clu
Gm128
B2m
Hspa2
Spesp1
Calm1
padj < 0.05
−log10 p−value
log2 fold change
Prm2Δc/- vs. WT
Gm128
Spesp1
Calm1
B2m
Clu
Eef1a2
H2al2a
padj < 0.05
−log10 p−value
log2 fold change
B
Differential abundance analysis overlap
Prm2Δc/+ vs. WT
Tuba3
Cs
Slc25a31
Gpd2
Gstm5
Prm2Δc/- vs. WT
Spesp1
Hspa2
Gm128
B2m
Calm
Clu
Eef1a2
H2al2a (H2A.L.2)
4933411K16Rik
Rpl26
Prm2-/- vs. WT
2
3
2
7
3
7
8
C
H2A.L.2 abundance
median-normalized log2 abundance
WT
Prm2-/-
Prm2Δc/+
Prm2Δc/-
D
Database network
PRM2
PRM1
TNP1
TNP2
H2A.L.2

Fig. 6

H2A.L.2 and PRM2 IHC

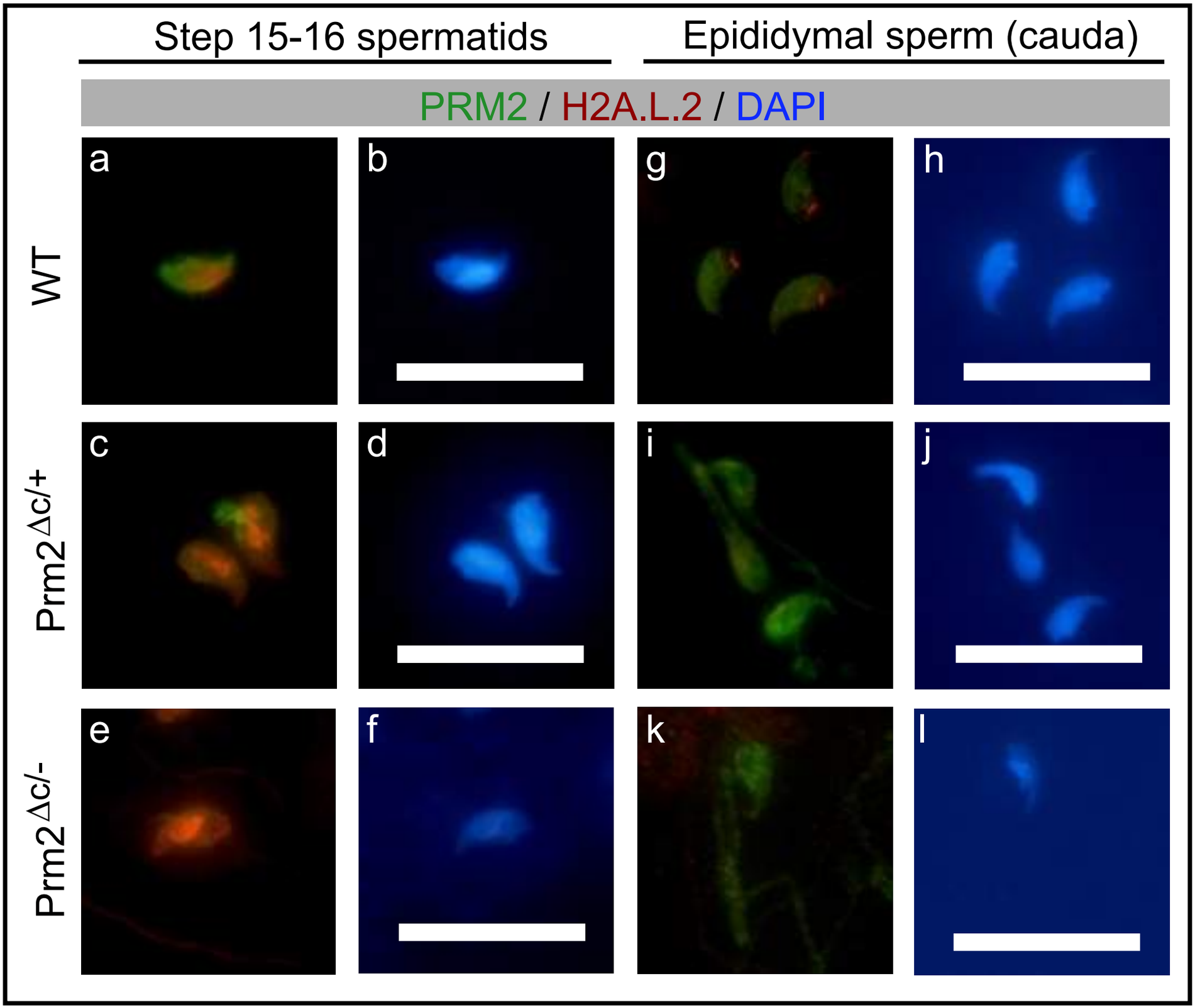

Fig. 7